Astron. Nachr. / AN **333**, No. , 1 – 9 (2012) / **DOI** ***please set DOI!***

The spectroscopic orbit of the K-giant binary γ Canis Minoris*

Francis C. Fekel[1 ⋆⋆◦], **Michael H. Williamson**[1], **Michael Weber**[2], **Klaus G. Strassmeier**[2], **Dimitri Pourbaix**[3]

[1] Center of Excellence in Information Systems, Tennessee State University (TSU), 3500 John A. Merritt Boulevard, Box 9501, Nashville, Tennessee 37209, U.S.A.
[2] Leibniz-Institute for Astrophysics Potsdam (AIP), An der Sternwarte 16, D-14482 Potsdam, Germany
[3] FNRS Senior Research Associate, Institut d'Astronomie et d'Astrophysique, CP 226, Universite Libre de Bruxelles, Boulevard du Triomphe, B-1050 Bruxelles, Belgium

Received 2012, accepted 2012
Published online 2012

Key words binaries: spectroscopic – stars: individual: γ CMi – stars: late-type – techniques: radial velocities

We have determined an improved orbit for the bright, evolved, double lined binary γ Canis Minoris. The system has an orbital period of 389.31 days and an eccentricity of 0.2586. We have revised the secondary to primary mass ratio to 0.987. The spectral types of the primary and secondary are K4 III and K1: III, respectively, and the components have a V magnitude difference of 2.2. Orbital fits to the *Hipparcos* astrometry are not definitive but suggest an orbital inclination of $\sim 66^\circ$, which produces masses of 1.88 and 1.85 $M_\odot$ for the components. A comparison with evolutionary tracks results in an age of 1.3 Gyr. STELLA very low amplitude radial velocity residuals of the secondary indicate a period of 278 days. We interpret this as the rotation period of the secondary, detectable because of star spots rotating in and out of view. This period is nearly identical to the pseudosynchronous rotation period of the star. The primary is rotating more slowly than its pseudosynchronous rate.

1 Introduction

The bright star γ CMi = HR 2854 = HD 58972 (α = $7^h28^m9.79^s$, δ = $8°55'31.9''$; 2000.0) was announced as a velocity variable by Reese (1902) from observations obtained at Lick Observatory. Over three decades later Christie (1934) computed a single-lined binary orbit, which had an orbital period of 389 days. More than a half century passed before Scarfe (1995) reported the discovery of the lines of the secondary. Having accumulated an extensive set of radial velocities at the Dominion Astrophysical Observatory (DAO), Scarfe (2008) published substantially improved orbital elements for the double-lined spectroscopic binary, determining a period of 389.32 days. He concluded that although both components are late-type evolved stars that are similar in mass, having a secondary to primary mass ratio of 0.903, they are very different in luminosity.

Roman (1952) classified the star as K3 III and Keenan & McNeil (1989) more recently assigned it the identical spectral type but also noted that its spectrum was metal deficient relative to the Sun. This has been quantitatively confirmed by the abundance results of Brown et al. (1989) and McWilliam (1990). However, neither of those two results accounted for the binary secondary detected by Scarfe (1995, 2008).

McAlister (1976) estimated that γ CMi could have a maximum angular separation of 28 mas, while Halbwachs (1981) predicted a similar value of 31 mas. Thus, in searching for bright binary field stars that might be resolved by interferometry, we began observing γ CMi at TSU/Fairborn in 2005. Our interest intensified with Scarfe's (2008) characterization of the secondary as a late-type evolved star, and we decided to make a coordinated TSU/Fairborn and AIP/Tenerife observing campaign. Our new observations and data reductions are described in Sect. 2 and Sect. 3. In Sect. 4, we report on an improved orbital solution for γ CMi and in Sect. 5 examine the velocity residuals. In Sects. 6 and 7 we discuss the system's properties based on the new orbit. We then reanalyze the *Hipparcos* intermediate astrometric data in Sect. 8 and examine the evolutionary status of the sytem.

2 Observations

2.1 Fairborn Observatory

From 2005 March through 2012 February, we collected 144 usable observations with the Tennessee State University 2 m automatic spectroscopic telescope (AST) and fiber-fed echelle spectrograph, which is situated at Fairborn Observatory near Washington Camp in the Patagonia Mountains

* Based partly on data obtained with the STELLA robotic telescope in Tenerife, an AIP facility jointly operated with IAC.

** Visiting Astronomer, Kitt Peak National Observatory, National Optical Astronomy Observatory, operated by the Association of Universities for Research in Astronomy, Inc. under a cooperative agreement with the National Science Foundation.

◦ Corresponding author: fekel@evans.tsuniv.edu

Table 1 Fairborn Observatory radial velocities of γ CMi. The full table of 144 velocity pairs is available electronically.

HJD -2450000	Orb. Phase	V_1	(O-C)$_1$ (km s^{-1})	V_2	(O-C)$_2$
3430.869	0.200	31.7	−0.6	59.5	−0.3
3443.750	0.233	35.8	−0.4	54.9	−1.0
3456.792	0.267	39.7	−0.3	51.4	−0.7
3512.645	0.410	52.9	−0.0	38.6	−0.4
3666.041	0.804	57.6	+0.1	35.3	+1.0
3680.996	0.843	53.3	+0.0	39.0	+0.4
3723.065	0.951	33.7	−0.2	56.8	−1.5
3735.852	0.984	27.6	+0.1	64.5	−0.2
3748.897	0.017	22.4	−0.4	68.8	−0.7
3762.857	0.053	20.2	−0.3	71.8	−0.0

Table 2 STELLA observatory radial velocities of γ CMi. The full table of 241 velocity pairs is available electronically.

HJD -2450000	Orb. Phase	V_1	(O-C)$_1$ (km s^{-1})	V_2	(O-C)$_2$
54779.680	0.665	62.938	+0.034	28.924	+0.065
54781.703	0.670	62.925	+0.026	28.878	+0.013
54788.725	0.688	62.817	+0.030	29.008	+0.030
54794.721	0.703	62.590	+0.019	29.201	+0.004
54798.520	0.713	62.388	+0.017	29.380	−0.019
54806.499	0.734	61.783	+0.005	29.973	−0.027
54806.503	0.734	61.780	+0.002	29.988	−0.012
54807.510	0.736	61.688	+0.003	30.069	−0.025
54809.497	0.741	61.491	+0.001	30.234	−0.058
54817.494	0.762	60.513	−0.015	31.290	+0.022

of southeastern Arizona. During the first six years of observing, from 2005 March through 2011 April, the detector was a 2048×4096 SITe ST-002A CCD. Those echelle spectrograms have 21 orders that cover the wavelength range 492–710 nm. Before 2010 January the spectra had a resolution of 0.017 nm, while afterward the resolution decreased to 0.024 nm, the corresponding resolving powers are R = 35,000 and 25,000, respectively. In the summer of 2011 the SITe CCD detector and dewar were replaced by a Fairchild 486 CCD, having 4K×4K 15 μm pixels, that was housed in a new dewar. The echelle spectrograms that were obtained with this new detector have 48 orders, covering the wavelength range 380 nm–826 nm. The observation exposure time for the first four years was generally 300 s but was reduced to 240 seconds during the last three years. Typical signal-to-noise (S/N) ratios of the spectra are $\sim$150 at 600 nm.

2.2 STELLA/SES

From 2008 November to 2012 March, a total of 241 spectra were obtained with the 1.2 m robotic STELLA-I telescope. Together with STELLA-II, STELLA-I makes up the AIP/STELLA Observatory on the island of Tenerife (Strassmeier et al. 2004, 2010). The fiber-fed STELLA Echelle Spectrograph (SES) is the telescope's only instrument. It is a white-pupil spectrograph with an R2 grating with two off-axis collimators, a prism cross disperser and a folded Schmidt camera with an E2V 2K×2K CCD as the detector. All spectra have a fixed format on the CCD and cover the wavelength range from 388–882 nm with increasing inter-order gaps near the red end from 734 nm to 882 nm. Of the total of 82 echelle orders, 62 are used for scientific analysis. The resolving power is R=55,000 corresponding to a spectral resolution of 0.012 nm at 650 nm. For γ CMi the exposure time was set to 300 s until the end of 2009 and to 200 s thereafter. This produced S/N ratios between 300 and 100, depending on weather conditions. Further details of the performance of the telescope and spectrograph system were reported by Weber et al. (2008) and Granzer et al. (2010).

2.3 Kitt Peak National Observatory

From 2009 to 2010, we acquired 5 red wavelength observations of γ CMi with the Kitt Peak National Observatory (KPNO) coudé feed telescope, coudé spectrograph, and a TI CCD detector. Those spectrograms are centered at 643 nm, cover a wavelength range of 8.4 nm, and have a resolution of 0.021 nm, corresponding to a resolving power of 30,000. The spectra have exposure times of 240 s and S/N ratios of about 250.

Table 3 DAO primary star radial velocities of γ CMi. The full table of 117 velocities is available electronically from CDS.

HJD -2400000	Orbital Phase	V_1	$(O-C)_1$ (km s^{-1})
43215.710	0.961	32.3	+0.5
43550.823	0.822	56.3	+0.5
44257.813	0.638	62.1	−0.7
44264.844	0.656	63.5	+0.6
44291.778	0.725	62.6	+0.5
44321.751	0.802	58.2	+0.5
44614.845	0.555	61.0	+0.2
44639.841	0.619	62.7	+0.2
44670.646	0.698	62.9	+0.2
44707.747	0.793	59.3	+0.9

3 Spectrum reduction and velocity analysis

3.1 Fairborn Observatory

Eaton & Williamson (2007) have given a description of the TSU 2 m telescope and spectrograph, operated at Fairborn Observatory near Washington Camp in the Patagonia Mountains of southeastern Arizona. They also have extensively described the echelle spectrum reduction.

For the Fairborn Observatory spectrograms a revised solar line list with lines that were more suitable for K giant stars was chosen for measurement of the radial velocities. This list comprised 63 regions between 492 nm and 710 nm, centered on the rest wavelengths (Moore et al. 1966) of relatively strong, mostly Fe I lines that were not extensively blended with other nearby strong features. Lines at the ends of each echelle order were excluded because of their lower signal-to-noise ratios. The wavelength scale of each spectrum was initially determined from Th–Ar comparison spectra that were obtained at the beginning and end of the night, and that scale was refined with the use of the telluric O_2 lines near 690 nm, which are in each stellar spectrum. An empirical profile that was rotationally broadened by shifting and adding the profiles together after weighting them by the limb darkening adopted for the Sun was used to fit the lines. For the velocities of blended components two rotational broadening functions were used to reproduce the combined profile. The difference between the observed wavelength, determined from the rotational broadening fit, and that given in the solar line list of Moore et al. (1966) was used to compute the radial velocity, and a heliocentric correction was applied. From the individual lines a mean velocity for each component was determined. Thus, the resulting Fairborn velocities are absolute velocities.

Our unpublished measurements of several IAU standard solar-type stars indicate that the Fairborn Observatory velocities from the SITe CCD have a small zero-point offset of -0.3 km s^{-1} relative to the velocities of Scarfe (2010). Thus, we have added 0.3 km s^{-1} to each of those Fairborn velocities. Similarly, we have determined that the velocities that have been obtained with the Fairchild CCD have a zero-point offset of -0.6 km s^{-1} relative to those of Scarfe (2010). Thus, 0.6 km s^{-1} has been added to each of those velocities. The Fairborn Observatory observations and radial velocities are listed in Table 1.

3.2 STELLA/SES

SES spectra are automatically reduced with the IRAF[1]-based STELLA data-reduction pipeline (Weber et al. 2008). The images were corrected for bad pixels and cosmic-ray impacts. Bias levels were removed by subtracting the average overscan from each image followed by the subtraction of the mean of the (already overscan subtracted) master bias frame. The target spectra were flattened by dividing by a nightly master flat which has been normalized to unity. The nightly master flat itself is constructed from approximately 50 individual flats observed during dusk, dawn, and around midnight. After removal of the scattered light, the one-dimensional spectra were extracted with the standard IRAF optimal extraction routine. Wavelength calibration was done with consecutively recorded Th-Ar spectra. Finally, the extracted spectral orders were continuum normalized with the use of flux-normalized synthetic spectra of the same spectral classification as the target in question.

[1] The Image Reduction and Analysis Facility is hosted by the National Optical Astronomy Observatories in Tucson, Arizona at URL iraf.noao.edu.

STELLA radial velocities are determined from an order-by-order cross correlation with a synthetic template spectrum from an ATLAS-9 atmosphere (Kurucz 1993) that roughly matches the component spectral classification. In the case of γ CMi, a two-dimensional cross correlation was performed to extract primary and secondary velocities simultaneously. A weighted average of the 62 individual correlation images gives a single radial velocity pair. The cross-correlation templates were constructed with $T_{\rm eff} = 4250$ K, $\log g$ =2.0, solar abundance, $v \sin i = 5\,{\rm km\,s^{-1}}$, a macroturbulence $\zeta = 4.4\,{\rm km\,s^{-1}}$, and K3 III as a flux template for the primary component, and $T_{\rm eff} = 4500$ K, $\log g$ =4.0, solar abundance, $v \sin i = 4\,{\rm km\,s^{-1}}$, $\zeta = 1.5\,{\rm km\,s^{-1}}$ and K2 V as flux template for the secondary star. For the intensity ratio, we used 6.6. The 241 least blended STELLA observations and radial velocities are given in Table 2. Numerical simulations of the cross correlation errors with synthetic spectra were discussed by Weber & Strassmeier (2011). These were applied to all STELLA γ CMi velocities. Note that the best achieved external rms value of a single measurement is 30 m s^{-1} (for 51 Peg, a sharp-lined, late-type single star). The STELLA radial velocities are barycentric and corrected for the Earth's rotation. No gravitational redshift correction is applied.

Strassmeier et al. (2012) analyzed observations of 22 radial velocity standard stars obtained with the same set-up as in this paper. The STELLA/SES system appears to have a zero-point offset of +0.503 km s^{-1} with respect to the CORAVEL system (Udry et al. 1999). The STELLA observations and radial velocities are listed in Table 2.

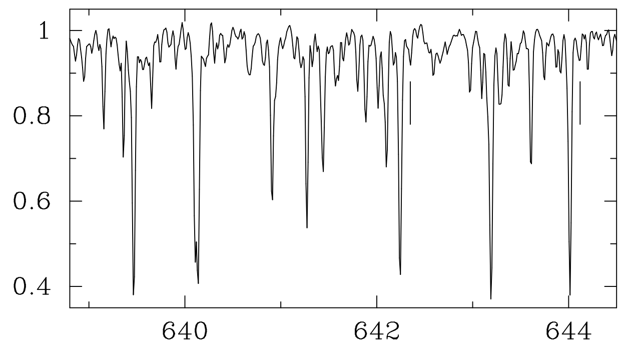

Fig. 1 KPNO spectrum of γ CMi in the 642 nm wavelength region obtained near one of the nodes in the orbit. The y-axis is relative intensity. Tick marks at 642.35 and 644.12 nm identify two of the least blended, redshifted, secondary star lines in this wavelength region.

3.3 Kitt Peak National Observatory

The single-order KPNO spectra were reduced with standard IRAF routines. As noted previously, those observations have a very limited wavelength coverage of just 8.4 nm. This small wavelength range, the weakness of even the strongest secondary features, and the very numerous lines

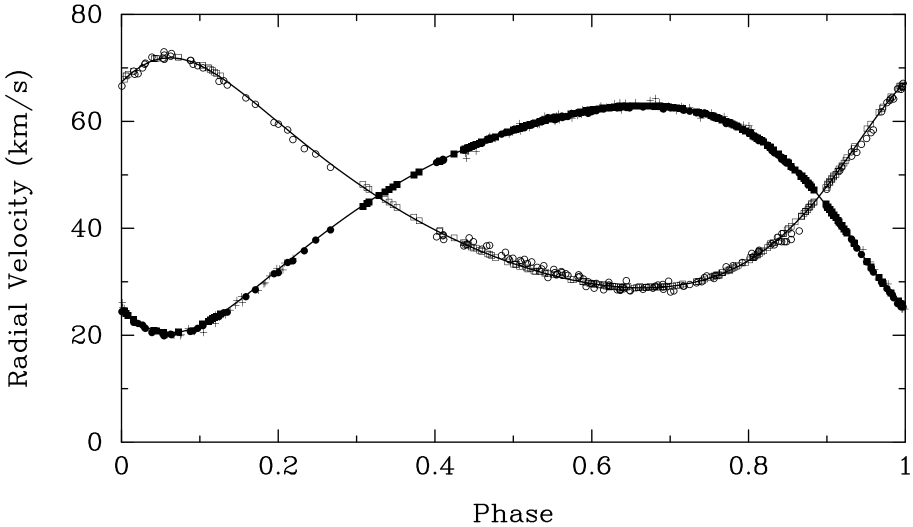

Fig. 2 Radial velocities of γ CMi compared to the computed radial velocity curves. Zero phase is a time of periastron. Solid circles: Fairborn primary, Solid squares: STELLA primary, Pluses: DAO primary, Open circles: Fairborn secondary, Open squares: STELLA secondary.

of the mid-K spectral class primary, conspire to produce secondary lines in the 643 nm wavelength region that are extensively blended with weak primary features, even when the secondary lines are near maximum separation from the primary lines (Fig. 1). While precise velocity measurements of the primary component can be obtained in these spectra, the velocity measurement of the secondary lines in our spectra is compromised. Because they are few in number and are combined with weak lines of the primary, the resulting average velocity from those lines is poorly determined and affected by the blends. Thus, given the small number of KPNO spectra, velocities from them have not been included in our solution.

4 New orbit determinations

Having three extensive sets of radial velocities, those from the DAO, the Fairborn Observatory, and the STELLA Observatory, we computed six independent sets of elements, three for each component, with the spectroscopic binary orbit program SB1 (Barker et al. 1967), which obtains a solution by differential corrections. Our analysis of the DAO data (Scarfe 2008) excluded 31 observations with very blended components (The observations used in the final global solution, determined below, are reprinted in Table 3). The period determined from the solution of each set of primary velocities was adopted for the corresponding solution of each set of secondary velocities. Table 4 lists the orbital periods, the center-of-mass velocities, and the semiamplitudes of the primary and secondary from the six solutions.

As shown in Table 4, the center-of-mass velocities of the primary that were determined from the three velocity data sets are in excellent agreement, having a maximum difference of only 0.18 km s^{-1}. From the variances of the separate orbital solutions, the STELLA, Fairborn, and DAO velocities of the primary were assigned weights of 1.0, 0.3, and 0.03, respectively. Similarly, the STELLA, Fairborn, and DAO velocities of the secondary, were given weights of 0.4, 0.02, and 0.005. We then used the 502 appropriately weighted velocities of the primary to obtain an orbital solution that produced a period of 389.305 $\pm$ 0.011 days. This period is 0.2 days shorter than that found by the STELLA primary velocities alone (Table 4) but is very similar that that found by Scarfe (2008).

To confirm the validity of the shorter period, we also computed two orbital solutions for the Lick Observatory observations (Christie 1934), which were begun 112 years ago. We used 18 of the 19 velocities (one value with a large residual was given a weight of zero) and first adopted the STELLA-Fairborn-DAO period of 389.31 days and then the STELLA period of 389.50 days. The Lick velocities phase very well with the orbital period determined from the combined three observatory data, but when phased with the STELLA period, the velocities are systematically shifted in phase by about 0.05 and the sum of the residuals squared increases by nearly a factor of three relative to the previous solution with the shorter period.

Finally, we obtained a combined solution of the DAO, Fairborn, and STELLA velocities of the primary and the Fairborn and STELLA velocities of the secondary. The DAO secondary velocities were not included in the solution because their semiamplitude differs by nearly 10% from that of the other two data sets. Scarfe (private communication, 2012) has reported that although great care was taken to remove secondary velocities from his orbital solution that might have been compromised (see Scarfe et al. 2007 and their Fig. 1 for a general discussion of the problem), the radial velocity scanner, which was used to obtain nearly all the DAO observations of γ CMi, produces a velocity trace that might still have some systematic effects for the very

Table 4 Orbital elements from single-lined solutions.

Parameter	Primary Component DAO	Fairborn	STELLA	Secondary Component DAO	Fairborn	STELLA
P (days)	389.35	389.25	389.50	389.35	389.25	389.50
	$\pm$ 0.03	$\pm$ 0.04	$\pm$ 0.01	(adopted)	(adopted)	(adopted)
γ (km s^{-1})	45.96	45.79	45.970	45.20	45.91	46.14
	$\pm$ 0.06	$\pm$ 0.02	$\pm$ 0.003	$\pm$ 0.24	$\pm$ 0.07	$\pm$ 0.01
K (km s^{-1})	21.42	21.34	21.231	23.70	21.36	21.63
	$\pm$ 0.07	$\pm$ 0.02	$\pm$ 0.004	$\pm$ 0.23	$\pm$ 0.08	$\pm$ 0.01

Table 5 Spectroscopic orbital elements and related quantities.

Parameter	Scarfe (2008)	This study
P (days)	389.322 $\pm$ 0.016	389.310 $\pm$ 0.012
T (HJD)	2449848.2 $\pm$ 0.8	2449849.172 $\pm$ 0.089
e	0.259 $\pm$ 0.004	0.25856 $\pm$ 0.00039
ω_1 (deg)	139.6 $\pm$ 0.8	142.079 $\pm$ 0.090
K_1 (km s^{-1})	21.41 $\pm$ 0.07	21.243 $\pm$ 0.010
K_2 (km s^{-1})	23.73 $\pm$ 0.18	21.526 $\pm$ 0.017
γ (km s^{-1})	45.86 $\pm$ 0.05	45.9947 $\pm$ 0.0061
$a_1 \sin i$ (10^6 km)	110.7 $\pm$ 0.4	109.852 $\pm$ 0.055
$a_2 \sin i$ (10^6 km)	122.7 $\pm$ 0.9	111.320 $\pm$ 0.089
$M_1 \sin^3 i$ (M$_\odot$)	1.76 $\pm$ 0.03	1.4317 $\pm$ 0.0022
$M_2 \sin^3 i$ (M$_\odot$)	1.59 $\pm$ 0.02	1.4129 $\pm$ 0.0017
M_2/M_1	0.903 $\pm$ 0.007	0.9868 $\pm$ 0.0009
Standard error of a unit weight velocity (km s^{-1})	...	0.11

low contrast profiles of the secondary. Given their very low weights, inclusion of the DAO velocities of the secondary would produce very little change in the combined solution.

The orbital elements and related quantities from our double lined solution are listed in Table 5 and compared with the results of Scarfe (2008). The orbital periods and most other elements of the two solutions are in very good agreement, and most uncertainties have been improved by about an order of magnitude in the new solution. However, as a result of the significantly smaller secondary velocity semiamplitude, the newly determined mass ratio of the components is much closer to unity than Scarfe's value. The radial velocities are compared with the computed velocity curves in Fig. 2. The phases and velocity residuals of the velocities are given as part of Tables 1,2, and 3.

5 Velocity residuals

The three orbital solutions of the primary from the DAO, Fairborn, and STELLA radial velocities, respectively, show no evidence of systematic residuals. However, the situation for the Fairborn and STELLA velocities of the secondary component is rather different.

From the orbital solution of the Fairborn velocities of the secondary, we examined a plot of the velocity residuals versus phase. This plot showed that most of the Fairborn secondary velocities in certain phase ranges are systematically shifted toward the center-of-mass velocity. The resolution of the Fairborn spectra is substantially lower than that of the STELLA spectra, and this lower resolution may be at least partially to blame for the systematic shift of the Fairborn velocities. These residuals however do not significantly affect the semiamplitude of the secondary, which differs from that of the STELLA secondary velocity solution by just 1%. A period search of the residuals produces a weak period at 96 days, which we believe has no physical significance.

An orbital solution of the STELLA velocities of the secondary shows that they also have systematic residuals but with a much much smaller amplitude than that of the Fairborn data. An analysis of the residuals with a sine curve finds a mathematically significant variation with a period of 278 $\pm$ 2 days and a semiamplitude of 111 m s^{-1} (Fig. 3). These velocity residuals may well have a physical cause, and that possibility is examined in Sect. 8.

6 Spectral types and magnitude difference

To determine spectral types of late-type stars, Strassmeier & Fekel (1990) identified several luminosity-sensitive and temperature-sensitive line ratios in the 643–646.5 nm region. Those line ratios plus the general appearance of the spectrum were employed as spectral-type criteria.

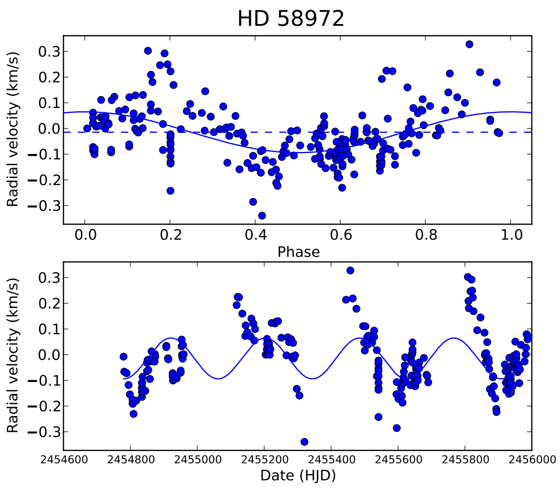

Fig. 3 STELLA velocity residuals of the secondary phased with a period of 287 days and compared with our sine curve fit (Top panel). STELLA residuals versus Julian date compared to our sine curve fit (Bottom panel).

Keenan & McNeil (1989) classified γ CMi as a K3 III and added an abundance index classification of Fe-1 to indicate that the star is metal weak relative to the Sun. Quantitative abundance analyzes that have been carried out by Brown et al. (1989) and McWilliam (1990) lead to a mean calibrated abundance of [Fe/H] = -0.409 ± 0.084 (Taylor 1999). However, this measured underabundance relative to the Sun at least partially results from the continuum of the secondary, which weakens the true line strengths of the much more easily visible primary.

A KPNO spectrum of γ CMi, obtained when the components were near a nodal separation, was compared with the spectra of a number of G and K subgiants and giants from the list of Keenan & McNeil (1989). The reference star spectra were obtained at KPNO with the same telescope, spectrograph, and detector as our γ CMi spectrum. To facilitate a comparison, various combinations of the reference-star spectra were rotationally broadened, shifted in radial velocity, appropriately weighted, and added together with a computer program developed by Huenemoerder & Barden (1984) and Barden (1985) in an attempt to reproduce the composite spectrum of the binary.

The reference stars β Cnc (K4 III; Keenan & McNeil 1989 and mean [Fe/H] = -0.13 (Taylor 1999)) and ϵ CrB (K2 IIIab; Keenan & McNeil 1989 and mean [Fe/H] = -0.17 (Taylor 1999)) produce a very good fit to the primary and secondary, respectively. A very similar fit results from replacing the secondary with ϵ Cyg (K0 III; Keenan & McNeil 1989 and mean [Fe/H] = -0.18 (Taylor 1999)). Stars with spectral types of G7 III and K4 III provide significantly poorer fits to the secondary. Thus, we assign spectral types of K4 III and K1: III for the primary and secondary, respectively. The colon indicates the greater uncertainty in the spectral class of the secondary that results because of its very weak lines. The stars are slightly metal poor relative to the Sun.

The continuum intensity ratio of the secondary/primary is 0.111, which results in a continuum magnitude difference of 2.4 mag at 643 nm. The secondary has a similar spectral class to that of the primary, and the 643 nm region is about 0.6 of the way between the V and R band passes, so we adopt a slightly smaller V difference of 2.2 mag and estimate an uncertainty of 0.2 mag.

7 Basic Properties

To determine the basic properties of γ CMi, we use the Stefan-Boltzmann law. We begin by adopting a V magnitude and $B - V$ color from the *Hipparcos* catalog (ESA 1997), which are 4.33 and 1.43, respectively. With our V magnitude difference of 2.2 the apparent V magnitudes of the individual components become 4.46 and 6.66. The new *Hipparcos* parallax reduction by van Leeuwen (2007) results in a value of 10.25±0.47 mas and corresponds to a distance of 97.6±4.5 pc. At such a distance we assume that the system is unreddened. We then combine the apparent magnitudes and the parallax to obtain absolute magnitudes M_V = -0.5 ± 0.1 mag and M_V = 1.7±0.2 mag for the primary and secondary, respectively. We next adopt $B - V$ colors of 1.47 for the primary and 1.10 for the secondary. The latter is the value for a K1 III according to Johnson (1966), while the former is that value needed to reproduce the combined color of the system. Then from Table 3 of Flower (1996), we obtain the bolometric corrections and effective temperatures of the two components. The resulting luminosities of the primary and secondary are L_1 = 321±33 L$_\odot$ and L_2 = 25.4±5.2 L$_\odot$, respectively, while the radii are R_1 = 36.8±2.6 R$_\odot$ and R_2 = 7.8±1.0 R$_\odot$, respectively. The uncertainties in the computed quantities are dominated by the parallax uncertainty and to a lesser extent the effective temperature uncertainty with the latter estimated to be ±100 K for the primary and ±200 K for the secondary. The basic parameters of γ CMi are summarized in Table 6.

8 Discussion

As noted by Scarfe (2008), no eclipses have been published for γ CMi. From our minimum masses and orbital period we obtain a semimajor axis of 1.48 AU or 318 R$_\odot$ for the system. The revised *Hipparcos* parallax converts this into a semimajor axis of 15 mas. From the linear semimajor axis and our computed radii for the two components the upper limit of the inclination for no eclipses to occur is 82°.

Pourbaix & Boffin (2003) reanalyzed the *Hipparcos* intermediate astrometric data of a large number of binaries that contain a giant star. The γ CMi system was included in that analysis but was not one of the 29 systems that fulfilled a number of constraints on the reality of the derived orbits. As a result of our new spectroscopic solution, we

Table 6 Basic Parameters for γ CMi.

Parameter	Value	Reference
V (mag)	4.33	ESA 1997
$B-V$ (mag)	1.43	ESA 1997
Parallax (mas)	10.25 ± 0.47	van Leeuwen 2007
Spectral type (1)	K4 III	This study
Spectral type (2)	K1: III	This study
V_1 (mag)	4.46 ± 0.05	This study
V_2 (mag)	6.66 ± 0.2	This study
$M_{V,1}$ (mag)	-0.5 ± 0.1	This study
$M_{V,2}$ (mag)	1.7 ± 0.2	This study
$T_{\rm eff,1}$ (K)	4036 ± 100	This study
$T_{\rm eff,2}$ (K)	4658 ± 200	This study
L_1 ($L_\odot$)	321 ± 33	This study
L_2 ($L_\odot$)	25.4 ± 5.2	This study
R_1 ($R_\odot$)	36.8 ± 2.6	This study
R_2 ($R_\odot$)	7.8 ± 1.0	This study
M_1 ($i = 66°$) ($M_\odot$)	1.88	This study
M_2 ($i = 66°$) ($M_\odot$)	1.85	This study

reexamined the original as well as the revised *Hipparcos* data. The original *Hipparcos* data set contains 46 observations. Three solutions were examined. Fitting the observations with a single star model, produces no significant outliers and a goodness of fit of 1.25. Since that value is close to 1.0, the fit appears to be a good one. When Campbell's fit is adopted (i.e., the orbital elements ω, e, P, and T are fixed), the reduction of χ^2 with respect to the single-star value is very small and the orbital model is rejected, based on the F-test between the two solutions. With the Thiele-Innes fit, where only e, P, and T are assumed, the result is not substantially better but four outliers show up.

Once these four points are removed, the single star goodness of fit falls to -0.14. Once again, the Campbell fit does not yield a big improvement, producing the same conclusion from the F-test as that noted above. The same is true with the Thiele-Innes approach. Despite the lack of improvement with the use of an orbital fit to the data, the resulting astrometric solution is surprisingly consistent with the spectroscopic one because the argument of periastron, ω, is $142.3°$, which is in excellent agreement with the spectroscopic value of $142.1°$. The variable elements, the inclination and the position angle of the line of nodes, are very uncertain ($i = 65° \pm 15°$ and $\Omega = 109° \pm 14°$). This solution results in a parallax of 6.5±0.96 mas.

The revised data set of van Leeuwen, which he also fit with the single star model, contains 88 points. With one outlier removed the data were again constrained by the spectroscopic orbital elements. The Thiele-Innes fit results in an ω value of about $132°$, thus suggesting that the spectroscopic orbit might be barely detectable in the astrometric observations. A Campbell fit, where ω is fixed, results in an Ω of $96° \pm 3°$, and an inclination of $68° \pm 3.9°$. The resulting semimajor axis of the photocentric orbit is 3.2±0.13 mas and the parallax is 7.80±0.22 mas.

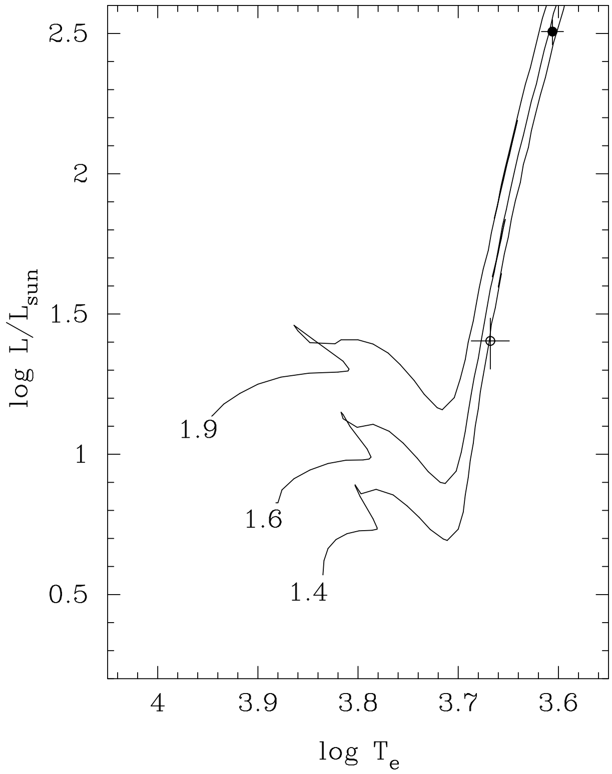

Fig. 4 Positions of the γ CMi primary (solid circle) and secondary (open circle) compared with the 1.4, 1.6, and 1.9 $M_\odot$ solar abundance evolutionary tracks of Girardi et al. (2000).

As a result of our new analyses, we conclude that the orbital wobble might be barely present in both the original and revised *Hipparcos* observations, but according to the criteria proposed by Pourbaix & Boffin (2003), the orbital solution should be discarded as too uncertain. However, we note that the orbital solutions, based on the two data sets, seem to favor an inclination of 65–68°, which is consistent with the lack of eclipses. Adopting an inclination of 66°, the masses become 1.88 and 1.85 $M_\odot$ for the primary and secondary, respectively. Those larger masses increase the angular semimajor axis slightly from 15 to 17 mas. With such a separation, the system can be resolved with interferometers such as CHARA or NPOI.

Scarfe (2008) determined a secondary to primary mass ratio of 0.903±0.007, which forced him to conclude that both components could not be on the first ascent giant branch at the same time. Thus, he postulated that the primary was in the core helium burning stage. Results from separate solutions of the STELLA data and the Fairborn Observatory data are much closer to unity. For STELLA the secondary to primary mass ratio from a simultaneous fit to the primary and secondary velocities is 0.9835 ± 0.0007, while for the Fairborn data the mass ratio is 1.006±0.004, making the fainter star slightly more massive. However, the semiamplitudes from the two Fairborn single-lined orbital solutions (Table 4) reverse the mass ratio, producing a value of 0.999. While the uncertainties do not enable the values of the mass ratios to overlap, the STELLA and Fairborn ratios are much closer to unity than Scarfe's value. Our secondary to primary mass ratio for the combined solution (Table 5) is 0.9868±0.0009. As mentioned earlier, there are systematic residuals in both new data sets. Even though the lower resolution Fairborn data is more likely to produce an erroneous result, we caution that the true uncertainty of the mass ratio value from the combined solution is likely to be larger than the formal result.

Scarfe et al. (2007) discussed HR 6046, a double-lined spectroscopic binary consisting of two late-type evolved stars of rather similar temperature but differing by an estimated 3.0 mag in V. They found a secondary to primary mass ratio of 0.988 and postulated that the two stars were on the first ascent giant branch. For giants of very unequal luminosity finding both stars in the first ascent phase should be a relatively rare phenomenon, given the small amount of time that a moderate mass star spends on the first ascent giant branch relative to the main sequence or the helium burning giant phase. Compared to HR 6046, the masses of the components of γ CMi are slightly more unequal, and the magnitude difference of γ CMi is smaller. We suggest that, like HR 6046, both components of γ CMi are on the first ascent giant branch.

In Fig. 4, we compare our effective temperatures and luminosities of the components with the solar abundance evolutionary tracks of Girardi et al. (2000). We have concluded that the stars are slightly metal poor, a result that would shift the evolutionary tracks to slightly higher temperatures. The positions of the stars are in better agreement with the tracks of somewhat lower mass stars, suggesting that the orbital inclination is higher than the value of 66° that we have adopted. The properties of the primary are much better determined than those of the secondary, and so we estimate an age for it of 1.3 Gyr from the evolutionary track of the 1.9 $M_\odot$ star.

The two main theories of orbital circularization and rotational synchronization (e.g., Zahn 1977, Tassoul & Tassoul 1992) disagree significantly on absolute time scales but do agree that synchronization should occur first. The eccentricity for the orbit of γ CMi is 0.259, and so circularization clearly has not yet occurred, but this is not surprising for a binary with an orbital period of 389 days.

In an eccentric orbit, Hut (1981) has shown that the rotational angular velocity of a star will tend to synchronize with that of the orbital motion at periastron. With equation (42) of Hut (1981), we compute a pseudosynchronous period of 277 days for γ CMi. From Table 6 the radii of 37 $R_\odot$ and 8 $R_\odot$ for the primary and secondary, respectively, and this period result in pseudosynchronous rotational velocities of 6.8 km s^{-1} for the primary and 1.5 km s^{-1} for the secondary.

The 278 day period found in the STELLA velocity residuals of the secondary is identical within its uncertainty to the predicted pseudosynchronous rotation period. This strongly suggests that, despite the small and variable amplitude, the velocity residuals are real. The most likely explanation is that the secondary has star spots that are strong enough to slightly distort the line profiles.

We have determined projected rotational velocities from our STELLA, KPNO, and Fairborn spectra with the procedure of Fekel (1997). Given the primary's relatively slow rotation, its $v \sin i$ value is dependent on the chosen macroturbulence. Adopting a macroturbulent velocity of 4 km s^{-1} from Massarotti et al. (2008) results in a $v \sin i$ value of 3.5 $\pm$ 1.0 km s^{-1} from the STELLA spectra and an average of 2.5 $\pm$ 1.0 km s^{-1} from the KPNO and Fairborn specta. Reducing the macroturbulent velocity to 3 km s^{-1} increases the $v \sin i$ values by about 1 km s^{-1}. Because of the weakness of the secondary lines and their blending with weak lines of the primary, the results for the secondary are much more problematic. With an adopted macroturbulence of 3 km s^{-1}, several lines of the secondary in the STELLA spectra result in a $v \sin i$ value of 5 $\pm$ 2 km s^{-1}, while from the Fairborn spectra we get a value of 2.0 $\pm$ 2.0 km s^{-1} for the secondary (the uncertainties are estimated). To convert the $v \sin i$ values into equatorial rotational velocities, we assume, as is generally done, that the axes of the orbital and rotational planes are parallel, so the inclinations are equal. An inclination of 66° increases the final averaged $v \sin i$ values to 3.3 and 3.8 km s^{-1} for the primary and secondary, respectively. Because of the large uncertainty in the secondary velocity, it is possible that the rotation of the secondary is pseudosynchronous, while the primary is clearly rotating more slowly than its pseudosynchronous value. Given the very rapid increase of the primary's radius as it quickly ascends the red giant branch, such a result should not be too surprising.

Future interferometric observations of this bright binary star, when combined with our spectroscopic observations, will lead to greatly improved basic parameters for the stars, including masses and an orbital parallax. Those results should enable a more robust comparison with theoretical evolutionary tracks.

Acknowledgements. We thank C. Scarfe for his useful comments on a preliminary version of this work. The research at Tennessee State University has been supported in part by NSF grant AST-1039522 and the state of Tennessee through its Centers of Excellence program. The STELLA facility is funded by the Science and Culture Ministry of the German State of Brandenburg (MWFK) and the German Federal Ministry for Education and Research (BMBF).

References

Barden, S. C. 1985, ApJ 295, 162
Barker, E. S., Evans, D. S., Laing, J. D. 1967, R. Obs. Bull. 130, 355
Brown, J. A., Sneden, C., Lambert, D. L., Dutchover, E. 1989, ApJS 71, 293
Christie, W. H. 1934, ApJ 80, 181
Eaton, J. A., Williamson, M. H. 2007, PASP 119, 886
ESA, 1997, The Hipparcos and Tycho Catalogues, ESA SP-1200, Noordwijk, ESA

Fekel, F. C. 1997, PASP, 109, 514
Flower, P. J. 1996, ApJ 469, 355
Girardi, L., Bressan, A., Bertelli, G., Chiosi, C. 2000, A&A 141, 371
Granzer, T., Weber, M., Strassmeier, K. G. 2010, Adv. in Astr. 2010, ID 980182
Halbwachs, J. L. 1981, A&AS 44, 47
Huenemoerder, D. P., Barden, S. C. 1984, BAAS 16, 510
Hut, P. 1981, A&A, 99, 126
Johnson, H. L. 1966, Ann. Rev. Astr. and Astrophys. 4, 193
Keenan, P. C., McNeil, R. C. 1989, ApJS 71, 245
Kurucz, R. L. 1993, ATLAS-9, CD-ROM #13
Massarotti, A., Latham, D. W., Stefanik, R. P., Frogel, J. 2008, AJ 135, 209
McAlister, H. A. 1976, PASP 88, 317
McWilliam, A. 1990, ApJS 74, 1075
Moore, C. E., Minnaert, M. G. J., Houtgast, J. 1966, *The Solar Spectrum 2935 Å to 8770 Å*, National Bureau of Standards Monograph 61, U.S. Government Printing Office, Washington, D. C.
Pourbaix, D., Boffin, H. M. J. 2003, A&A 398, 1163
Reese, H. M. 1902, Lick Obs. Bull. 1, 159:w
Roman, N. G. 1952, ApJ 116, 122
Scarfe, C. D. 1995, J. Royal Astron. Soc. Canada 89, 182
Scarfe, C. D. 2008, Observatory 128, 14
Scarfe, C. D. 2010, Observatory 130, 214
Scarfe, C. D., Griffin, R. F., Griffin, R. E. M. 2007, MNRAS 376, 1671
Strassmeier, K. G., Fekel, F. C. 1990, A&A 230, 389
Strassmeier, K. G., Granzer, T., Weber, M., et al. 2004, AN 325, 527
Strassmeier, K. G., Granzer, T., Weber, M. 2010, Adv. in Astr. 2010, ID 970306
Strassmeier, K. G., Weber, M., Granzer, T., Järvinen, S. 2012, AN submitted
Tassoul, J.-L., Tassoul, M. 1992, ApJ 395, 259
Taylor, B. J. 1999, A&AS 134, 523
Udry, S., Mayor, M., Maurice, E., Andersen, J., Imbert, M., Lindgren, H., Mermilliod, J.-C., Nordström, B., Prévot, L. 1999, in Hearnshaw, J.B. & Scarfe, C.D. (eds.), *Precise Stellar Radial Velocities*, IAU Colloq. 170, ASPC 185, p.383
van Leeuwen, F. 2007, A&A 474, 653
Weber, M., Granzer, T., Strassmeier, K. G., Woche, M. 2008, Proc. SPIE 7019, 70190L
Weber, M., Strassmeier, K. G. 2011, A&A 531, A89
Zahn, J.-P. 1977, A&A 57, 383